WORLD CONFERENCE ON TIMBER ENGINEERING 2025
BRISBANE, AUSTRALIA

Advancing Timber for the Future Built Environment

FINITE ELEMENT ANALYSIS OF REPLACEABLE STEEL PERFORATED PLATE FUSES IN TIMBER BRACED FRAMES

Yahia Ahmed[1], Hossein Daneshvar[2] , Ying He Chui[3]

ABSTRACT: Timber's inherent brittleness limits its use in seismic applications, particularly in tall buildings where ductility is essential. Timber-braced frames (TBFs) provide a potential solution, but current design codes lack specific guidance for their implementation. Unlike steel frames, timber bracing cannot rely on buckling to provide ductility, requiring effective connections to yield at the ends of braces. Incorporating yielding fuses, such as perforated steel plates, enhances ductility and localizes damage during seismic events. This study explores the utilization of perforated steel plates as seismic fuses in TBFs, focusing on flexural yielding mechanisms, specifically, long oval-shaped perforations. A numerical parametric study was conducted to evaluate various factors influencing the performance of these plates. The main findings indicate that increasing the slot length enhances peak deformation but reduces the plate's load capacity. However, increasing the number of link elements mitigates this loss. Combining the optimal slot length with an increased number of links achieved a 50% increase in peak deformation without compromising load capacity. This fuse design offers a promising strategy to improve the seismic resilience of timber-braced frames, as the steel plates can be replaced after a major seismic event without causing damage to the timber structure.

KEYWORDS: Timber Braced Frames (TBF), Seismic Force Resisting System (SFRS), Structural Fuse, Steel Perforated Plate, Finite Element Model (FEM).

1 INTRODUCTION

Despite the numerous advantages of timber, such as sustainability and ease of construction, its application in tall buildings remains limited due to its inherent brittleness, making it challenging to be utilized in applications that require ductile behavior. To address this limitation, incorporating ductile elements made from materials like steel is essential [1]. Timber-braced frames (TBFs) represent a promising solution. According to the National Building Code of Canada (NBCC) [2], using mass timber structures is now permitted up to 12 stories, with TBFs recognized as lateral load-resisting systems (LLRS) possessing moderate or limited ductility. For moderately ductile systems, the NBCC assigns a force modification factor (R_d) of 2.0 and an overstrength modification factor (R_o) of 1.5, while limited-ductility TBFs are assigned values of 1.5 for both factors.

Despite this acknowledgment in the NBCC, the Canadian Standard for Engineering Design in Wood (CSA O86-24) [3] currently lacks specific design guidance for TBFs. In contrast to steel-braced frames, which rely on buckling to provide ductility in compression, timber bracing members cannot depend on this mechanism due to the brittle nature of wood and its limited deformation capacity. Therefore, in TBFs, the connections at the ends of the braces play a critical role in achieving the required system ductility. By incorporating yielding fuses, ductility can be enhanced while damage is localized to specific structural elements during seismic events. Yielding fuses are particularly advantageous due to their simplicity and ability to generate broad hysteresis loops, facilitating high-energy dissipation [4].

A common method to induce yielding in steel is through perforations, a technique extensively studied in steel frames [5–9]. In this study, the fuses consist of perforated steel plates designed to form plastic hinges at the brace ends. These hinges protect timber elements by absorbing seismic forces and failing during seismic events, after which the fuses can be replaced without causing any damage to the timber elements. The application of perforated plates in timber construction has also been explored in previous research [10–13]. Daneshvar et al. [14] conducted comprehensive tests on these plates, followed by a parametric experimental study [15] investigating various perforation configurations. Their findings identified the elliptical perforation as the most effective shape for achieving high ultimate deformation. However, under cyclic loading conditions, a significant reduction in ultimate deformation, and hence in energy dissipation, was observed compared to monotonic tests.

[1] Yahia Ahmed, Department of Civil & Environmental Engineering, University of Alberta, Canada, helmiahm@ualberta.ca

[2] Hossein Daneshvar, Department of Civil & Environmental Engineering, University of Alberta, Canada, Hossein.daneshvar@ualberta.ca

[3] Ying-Hei Chui, Department of Civil & Environmental Engineering, University of Alberta, Canada, yhc@ualberta.ca

https://doi.org/10.52202/080513-0407

Another study [16] examined the failure mechanisms of these plates, using an experimental setup depicted in ***Figure 1*** (a). Two primary yielding mechanisms—shear and flexure—were identified. Among the tested configurations, the long oval perforation, illustrated in ***Figure 1*** (b), demonstrated a flexural yielding mechanism that provides the most promising performance. The primary aim of this study is to understand the fuse behavior better and potentially enhance the performance of flexure-yielding perforated plates through numerical investigations. This includes increasing the ultimate deformation and ductility of the connections, thus enhancing the seismic resilience of timber-braced frames.

(a) (b)

Figure 1.(a) Experimental test setup [16], (b) Long oval specimen [16]

2 METHODOLOGY

A numerical model was developed using the finite element (FE) software ABAQUS [17], employing three-dimensional solid geometries for analysis. Eight-node continuum linear hexahedral elements with reduced integration (C3D8R) were utilized throughout the simulations. To accurately capture the material behavior of the steel plates, six tensile coupon tests were conducted to determine their precise non-linear characteristics. Both elastic and plastic properties were incorporated into the model, simulating the steel plates with elastic-plastic behavior. This included the combined hardening effects of isotropic and kinematic hardening, along with cyclic hardening characteristics.

The finite element models (FEM) were developed to replicate the experimental boundary and loading conditions, as depicted in ***Figure 2*** (a). Both the experimental tests and FE simulations followed the ASTM E2126 Method C [18] cyclic loading protocol, to ensure consistency and comparability of results.

A mesh independence study was conducted to identify the optimal mesh configuration that balances accuracy and computational efficiency. The findings revealed that a 2 x 2 mm mesh for the perforated region and a 5 x 5 mm mesh for the rest of the plate provided optimum results. A sample of the meshing configuration is shown in ***Figure 2*** (b).

The FEM analysis employed a strain-based failure criterion defined by the equivalent plastic strain (PEEQ). This criterion was derived from the experimental results, indicating that the target strain aligns with a PEEQ value of 3.0, which was applied to simulate rupture initiation, as demonstrated in ***Figure 2*** (c). Following validation, a comprehensive parametric study was conducted to further enhance the performance of these fuses.

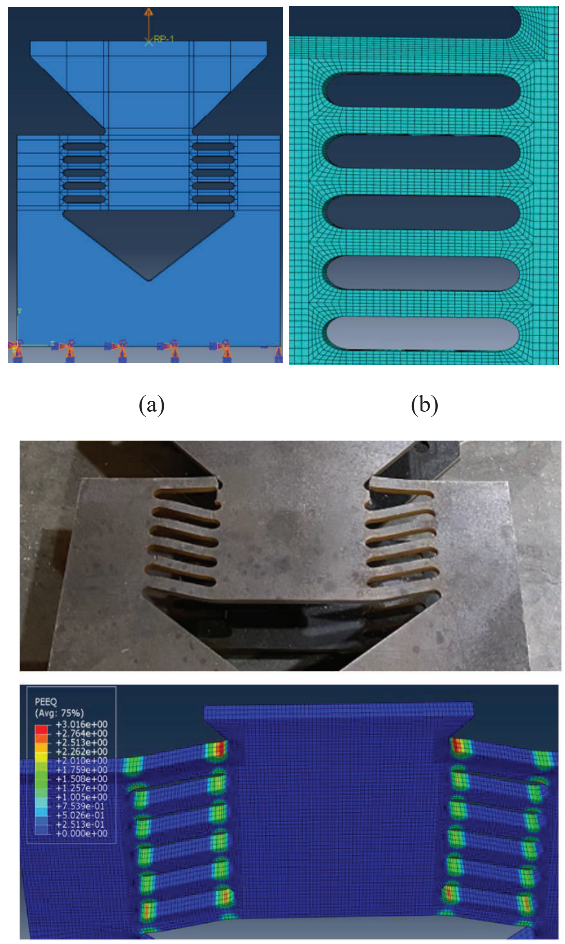

(a) (b)

(c)

Figure 2. (a) FEM boundary and loading conditions, (b) Mesh configuration, (c) Strain-based failure criterion (PEEQ=3.0).

2.1 FEM VALIDATION

The validation of the FEM began with a comparison of its hysteresis loops to the experimental results, as illustrated in ***Figure 3*** (a). Additionally, the backbone (or envelope) curves from both the numerical and experimental analyses were compared, revealing a positive deviation of approximately 15% and a negative deviation of around 5% in terms of energy dissipation. The equivalent energy elastic-plastic (EEEP) method [18] was applied to both cases, demonstrating a difference in energy dissipation of less than 10%, which was considered acceptable. Based on these findings, a validated FEM was established as a reference model for the following parametric study, focusing on varying a single parameter while keeping all others constant to accurately evaluate each parameter's effect on the plate's performance.

2.2 ASSESSMENT

A parametric study was conducted to enhance performance, with all FEM geometries presented in **TABLE 1** and ***Figure 3*** (b). the upper part of the connection which was attached to the glulam member, was designed as a capacity-protected dowel connection to ensure that all the deformation would occur within the perforation zone.

The EEEP method was a key technique for evaluating the results, estimating yield strength (P_{yield}) and elastic shear stiffness (K_e) using **Eq (1)** and **Eq (2)**, respectively:

$$P_{yield} = (\Delta_{ultimate} - \sqrt{(\Delta_{ultimate})^2 - \frac{2A}{K_e}})K_e \tag{1}$$

$$K_e = \frac{0.4P_{peak}}{\Delta_e} \tag{2}$$

Where (A) represents energy dissipation, and Δe is the deformation at 40% of the peak load. The ductility ratio (μ) is the ratio of the peak deformation over the yield deformation, and the over-strength factor (Ω) is determined by dividing the peak load by the yield load. The difference between ultimate and peak deformations was minimal, attributed to the limited post-peak response, as discussed in [14]. The EEEP results for all the FEMs utilized in this study are provided in **TABLE 2.**

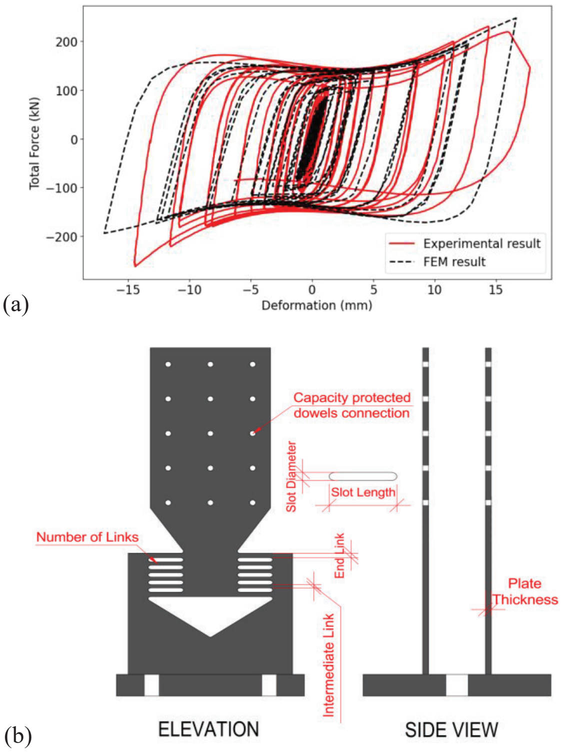

(a)

(b)

Figure 3.(a) Hysteresis loops for the Validation study,(b) FEM geometry

Table 1. FE Analysis Matrix.

FEM Label	Parameter Under Investigation	Plate Thickness (mm)	Link Element Geometry: No. of Links	Slot Dimension (mm x mm)	End Link width (mm)	Intermediate Link width (mm)
EBC-LO-1	**Reference specimen**	**12.5**	**6**	**10 x 57**	**10**	**7.5**
EBC-LO-2	**Plate Thickness**	**6.35**	6	10 x 57	10	7.5
EBC-LO-3		**19**	6	10 x 57	10	7.5
EBC-LO-4	**End Link Width**	12.5	6	10 x 57	**15**	7.5
EBC-LO-5		12.5	6	10 x 57	**7.5**	7.5
EBC-LO-6		12.5	6	10 x 57	**5**	7.5
EBC-LO-7	**Intermediate Link Width**	12.5	6	10 x 57	10	**10**
EBC-LO-8		12.5	6	10 x 57	10	**5**
EBC-LO-9	**Slot Length**	12.5	6	**10X65**	10	7.5
EBC-LO-10		12.5	6	**10X75**	10	7.5
EBC-LO-11		12.5	6	**10X85**	10	7.5
EBC-LO-12		12.5	6	**10X100**	10	7.5
EBC-LO-13		12.5	6	**10X110**	10	7.5
EBC-LO-14		12.5	6	**10X120**	10	7.5
EBC-LO-15	**Slot diameter (width)**	12.5	6	**7.5x57**	10	7.5
EBC-LO-16		12.5	6	**12.5x57**	10	7.5
EBC-LO-17		12.5	6	**15x57**	10	7.5
EBC-LO-18	**Number of Links**	12.5	**8**	10 x 57	10	7.5
EBC-LO-19		12.5	**4**	10 x 57	10	7.5
EBC-LO-20	**Enlarged slot length with an increase in the number of links**	12.5	**8**	**10X100**	10	7.5
EBC-LO-21		12.5	**9**	**10X100**	10	7.5
EBC-LO-22		12.5	**10**	**10X100**	10	7.5
EBC-LO-23		12.5	**12**	**10X100**	10	7.5

https://doi.org/10.52202/080513-0407

Table 2. Summary of FEM results

FEM Label	Parameter Under Investigation	Δ_{yield} (mm)	P_{yield} (kN)	Δ_{peak} (mm)	P_{peak} (kN)	A (kN.mm)	$K_{elastic}$ (kN/mm)	μ (mm/mm)	Ω (kN/kN)	No. of cycles completed to reach PEEQ 3
EBC-LO-1	**Reference specimen**	6.5 (-2.2)	190 (-144)	16.6 (-16.9)	247.1 (-193.9)	2630.9 (2394.9)	30 (66)	2.5 (7.7)	1.3 (1.3)	32
EBC-LO-2	**Plate Thickness**	2.8 (-2.5)	72.2 (-65.6)	9.7 (-9.5)	92.8 (-77.8)	636.2 (575.4)	25.5 (25.4)	3.5 (3.7)	1.3 (1.2)	16
EBC-LO-3		5.1 (-2.5)	339.2 (-269.5)	14.2 (-14.2)	436 (-341.2)	4278 (3548)	70 (106)	2.8 (5.6)	1.3 (1.3)	33
EBC-LO-4	**End Link Width**	1.8 (-1.8)	200 (-185)	11.9 (-11.5)	252 (-218)	2313 (2198)	112 (136)	6.8 (6.4)	1.3 (1.2)	29
EBC-LO-5		5.6 (-3.1)	192 (-149)	15.2 (-15.6)	251 (-215)	2878 (2587)	35 (50)	2.4 (4.5)	1.3 (1.3)	35
EBC-LO-6		7.6 (-5.1)	167 (-131)	17 (-16.8)	230 (-178)	2340 (1925)	22 (27.8)	2.2 (3.3)	1.4 (1.4)	35
EBC-LO-7	**Intermediate Link Width**	3.1 (-1.5)	225.8 (-188.9)	14.8 (-15)	303 (-240)	3122 (2997)	74.2 (122.8)	4.7 (9.9)	1.3 (1.3)	34
EBC-LO-8		7.1 (-4.2)	178 (-136.1)	15.4 (-15.2)	237 (-180.5)	2171 (1805.2)	44.5 (45.3)	2.2 (3.6)	1.3 (1.3)	34
EBC-LO-9	**Slot Length**	6.9 (-3)	158.1 (-121.5)	15.7 (-15.4)	207.4 (-160.5)	2042.3 (1746)	37.8 (40.9)	2.3 (5.2)	1.3 (1.3)	33
EBC-LO-10		7.7 (-5.1)	118 (-95)	17.1 (-16.2)	158 (-120.3)	1743 (1370)	25.6 (28.7)	2.2 (3.2)	1.3 (1.3)	36
EBC-LO-11		13.8 (-6.4)	153.3 (-105)	22.6 (-23.7)	194.5 (-140.9)	2479.4 (2252.1)	11.8 (17.1)	1.6 (3.7)	1.2 (1.3)	38
EBC-LO-12		8 (-6.5)	104.1 (-70)	25.6 (-24.8)	132.5 (-96)	1931 (1555.7)	7.4 (14.9)	3.2 (3.8)	1.2 (1.4)	41
EBC-LO-13		8.3 (-7.2)	90 (-72)	25.6 (-25.4)	127 (-99)	1928 (1615)	11.1 (11.6)	3.1 (3.5)	1.4 (1.4)	41
EBC-LO-14		14,3 (-9.5)	83 (-68)	25.5 (-25.7)	104 (-84)	1642 (1432)	10 (9.5)	1.8 (2.7)	1.3 (1.3)	4 3
EBC-LO-15	**Slot diameter (width)**	7.1 (-2.8)	185 (-138.1)	17.1 (-17)	240.9 (-184)	2644 (2240.8)	58.8 (66)	2.4 (6.1)	1.3 (1.3)	33
EBC-LO-16		6.9 (-2.7)	190 (-145.2)	17.1 (-17.2)	246.6 (-192)	2667 (2359)	42.5 (77.8)	2.5 (6.4)	1.3 (1.3)	33
EBC-LO-17		7 (-4.8)	175.3 (-132)	17 (-11.9)	243 (-156)	2673 (1460)	48.1 (-75.7)	2.4 (1.8)	1.4 (1.2)	32
EBC-LO-18	**Number of Links**	6.8 (-3.6)	227.7 (-188.8)	16.7 (-17)	282 (-233)	3324 (2880)	40 (54)	2.5 (4.7)	1.4 (1.2)	33
EBC-LO-19		7.5 (-4.5)	148 (-118.2)	16.8 (-17.2)	193.9 (-157)	2000 (1808)	39.8 (34.2)	2.2 (3.8)	1.3 (1.3)	34
EBC-LO-20	**Enlarged slot length with an increase in the number of links**	10.2 (-7.2)	122 (-104)	25.3 (-25)	154 (-127.4)	2607 (2282)	17.9 (16.7)	2.5 (3.5)	1.3 (1.2)	41
EBC-LO-21		7.3 (-9.5)	116 (-113.5)	24.8 (-25.4)	159.5 (-140)	2584 (2483)	16.6 (16.3)	3.4 (2.7)	1.3 (1.2)	41
EBC-LO-22		10.4 (-7.9)	132.4 (-119)	25 (-25)	167 (-140)	2864 (2624)	19 (19.1)	2.4 (2.7)	1.3 (1.2)	42
EBC-LO-23		10.1 (-7.9)	182.6 (-167.2)	25.1 (-25.5)	226 (-207)	3888 (3690)	30 (25)	2.5 (3.2)	1.2 (1.2)	41

3 PARAMETRIC STUDY RESULTS

3.1 PLATE THICKNESS

Firstly, a parametric study was conducted to evaluate the impact of plate thickness on the peak deformation of the perforated plate. EBC-LO-2, with a thickness of 6.35 mm, and EBC-LO-3, with a thickness of 19 mm, were compared to EBC-LO-1, which had a thickness of 12.5 mm, as illustrated in ***Figure 4*** (a). EBC-LO-2 endured only 16 cycles before experiencing global buckling, whereas EBC-LO-3 completed 33 cycles without any signs of buckling. It demonstrated superior energy dissipation and reduced peak deformation, with its ductility ratio decreasing by approximately 30% compared to the reference FEM (EBC-LO-1). The primary improvement observed was the increased peak load.

https://doi.org/10.52202/080513-0407

capacity of the plate, which reached 436 kN, the highest value among all FEMs.

3.2 END LINK WIDTH

As illustrated in ***Figure 2*** (c), failure initiates with the formation of plastic hinges at the end link locations. This highlighted the importance of investigating the effect of end link width. Four configurations—EBC-LO-1, 4, 5, and 6—were examined, with end link widths of 10 mm, 15 mm, 7.5 mm, and 5 mm, respectively, as shown by the hysteresis loops in ***Figure 4*** (b). Increasing the end link width altered the failure mode from a single plastic hinge at the end link to multiple hinges distributed throughout the intermediate links. However, this approach resulted in lower peak deformation, making it a less favorable solution.

3.3 INTERMEDIATE LINK WIDTH

EBC-LO-7 and EBC-LO-8, with intermediate link widths of 10 mm and 5 mm respectively, were compared to EBC-LO-1, which featured a width of 7.5 mm. The results, as shown in ***Figure 4*** (c), indicate that increasing the intermediate link width leads to higher energy dissipation and peak load capacity. However, it also results in a reduction in peak deformation. Among the tested configurations, EBC-LO-1 achieved the highest deformation while maintaining a balanced performance in terms of energy dissipation and peak load, making it the most optimal choice, for this parameter.

3.4 SLOT DIAMETER

A comparison of behavior across varying slot diameters is shown in ***Figure 4*** (d). The results indicate that this parameter has minimal influence on peak deformation or energy dissipation, as the hysteresis loops remain nearly identical. This suggests that the performance of the fuses is largely independent of the slot diameter.

3.5 SLOT LENGTH

One of the most impactful parameters in fuse performance is slot length. A parametric study was conducted on multiple FEMs with slot lengths ranging from 57 mm to 120 mm, as illustrated in ***Figure 4*** (e). The results show that as the slot length increases, the hysteresis loops become flatter, indicating higher peak deformation but reduced peak load and energy dissipation. This suggests that slot length is a promising parameter that warrants further investigation and optimization for improved performance.

3.6 NUMBER OF LINK ELEMENTS

Another crucial parameter is the number of link elements. ***Figure 4*** (f) compares the performance of configurations with 4, 6, and 8 link elements, all having the same slot size. The results reveal that increasing the number of links leads to higher peak load and greater energy dissipation. However, the peak deformation remains relatively consistent across the configurations, indicating that the increase in the number of links does not significantly affect the deformation capacity.

3.7 COMBINATION OF SLOT LENGTH AND NUMBER OF LINK ELEMENTS

Building on the insights from the previous two parameters, the authors of this study combined the effects of increased slot length and an increased number of links. This approach leverages the enhanced peak deformation associated with longer slots and the broader hysteresis loops and higher peak load achieved by increasing the number of links. As demonstrated in ***Figure 4*** (g), the combined configuration, represented by EBC-LO-23, achieved a 33% increase in peak deformation and a 32% increase in energy dissipation compared to EBC-LO-1. These results underscore the effectiveness of this combined strategy in improving the overall performance.

4 PARAMETRIC STUDY DISCUSSION

After completing the FE analyses and obtaining all results using the EEEP method, a post-processing analysis of the outcomes was performed for each parameter. This study aimed to identify which parameters significantly influenced the load-deformation behavior. The findings revealed the following key insights:

4.1 PLATE THICKNESS

This parameter was found to have a significant impact on altering the failure mode of the fuses, as illustrated in ***Figure 5*** (a). The EBC-LO-2 model, with a plate thickness of 6.35 mm, exhibited a failure mode shift from forming plastic hinges at the end links to global plate buckling. Although global buckling can contribute to energy dissipation, it is difficult to predict and should therefore be avoided.

On the other hand, the EBC-LO-3 model, with a plate thickness of 19 mm, exhibited increased stiffness, leading to a 16% reduction in peak deformation compared to the reference model. Based on these observations, the authors recommend using a plate thickness of 12.5 mm to achieve the desired flexural yielding behavior. Further studies are ongoing to explore the effects of additional plate thicknesses on fuse response.

4.2 END LINK WIDTH

Figure 5 (b), illustrates the effect of increasing the end link width on peak deformation. The results show that the difference in deformation is minimal when increasing the width from 5 mm to 10 mm. However, when the width reaches 15 mm, the deformation decreases significantly by approximately 30%. This reduction occurs because the yielding behavior shifts, distributing deformation throughout the intermediate links instead of concentrating at the end links. Consequently, energy dissipation also

https://doi.org/10.52202/080513-0407

decreases by a similar ratio. Among the tested configurations, the 10 mm end link width achieved the highest ductility ratio, with a value of 7.7.

Based on these findings, it is recommended to use an end link width of 10 mm to enhance the fuse performance in terms of peak deformation and energy dissipation.

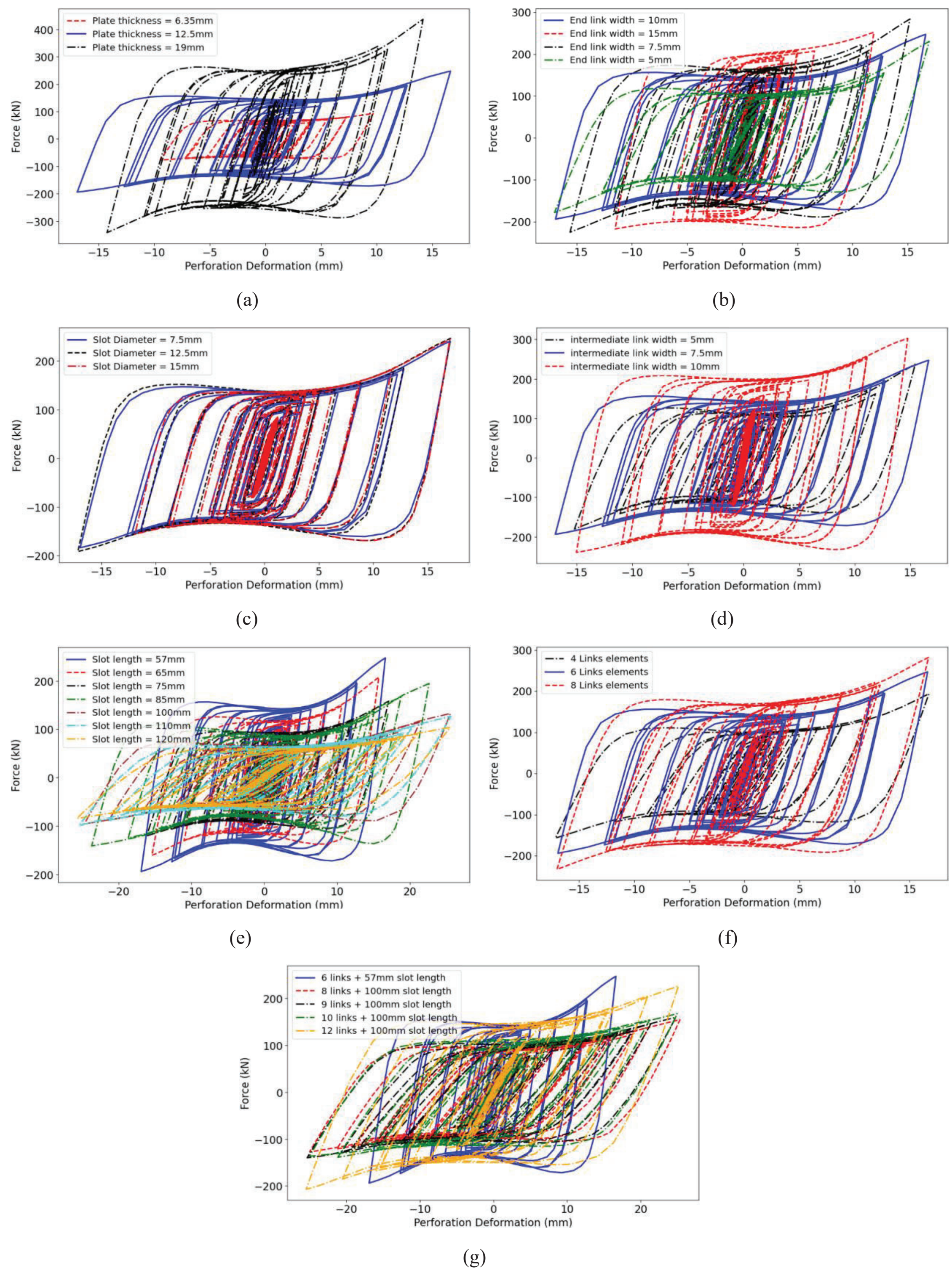

Figure 4. Load-displacement hysteresis loops comparisons considering different parameters:(a) plate thickness, (b) end link width, (c) intermediate link width, (d) slot diameter, (e) slot length, (f) number of links, (g) combination of slot length and number of links.

4.3 INTERMEDIATE LINK WIDTH

The results for this parameter are presented in ***Figure 5*** (c). The analysis indicates that this parameter has a negligible influence on the deformation capacity of the fuse. This outcome was expected, as most of the yielding and deformation occurs at the end link, with minimal contribution from the intermediate links in this failure mode. However, the authors suggest that future studies should focus on increasing the widths of the intermediate links, particularly in cases with wider end links. This adjustment could encourage all intermediate links to contribute more effectively.

4.4 SLOT DIAMETER

The slot diameter is an important parameter for perforated plates, as it influences stress concentration along the edges of the links. However, as shown in ***Figure 5*** (d), it has minimal impact on the deformation capacity for this particular perforated configuration. This is primarily because the design of this configuration focuses on achieving flexural yielding in the end link element. In contrast, for other configurations where the fuses are designed to yield in shear, the slot diameter would become a critical parameter, significantly affecting the results.

4.5 SLOT LENGTH

The slot length (perforation length) is one of the most effective parameters in this parametric study, as illustrated in ***Figure 5*** (e). Increasing the slot length from 57 mm to 100 mm resulted in a 52% increase in peak deformation. However, increasing the slot length beyond this point has diminishing effects as deformation becomes concentrated within the yielded zones of the link, and the plastic hinge length is already fully developed. Once the link's yielding capacity is maximized, further increases in slot length have minimal influence on additional deformation.

4.6 NUMBER OF LINK ELEMENTS

As previously noted, extending the slot length to 100mm was found to be effective. However, it resulted in a significant reduction in the peak load, which nearly halved. Consequently, the authors conducted an additional analysis using the same slot size (10mm x 100mm), but with an increased number of links, as shown in ***Figure 5*** (f). The results demonstrated that increasing the number of links from 5 to 12 led to a 37% increase in peak load. Furthermore, it was confirmed that the peak deformation remained consistent across all models, at approximately 25mm, since the slot length remained the same for all models. This approach effectively enhances peak deformation without compromising the plate load capacity

5 CONCLUSION

This study presents a numerical investigation into the flexural yielding behavior of perforated plates with a long oval shape, subjected to the ASTM E2126 Method C cyclic loading protocol. Following model validation, an extensive parametric analysis was performed, revealing that plate thickness plays a crucial role in determining failure modes. A thickness of 12.5 mm was found to provide the desired flexural yielding behaviour within the perforation zone.

To ensure the formation of a plastic hinge, the end link width should not exceed 10 mm. Other parameters, such as intermediate link width and slot diameter, were found to have minimal impact on performance for this configuration. Slot length emerged as the most effective factor in enhancing peak deformation, with optimal results observed at 100 mm. Additionally, increasing the number of link elements improves both energy dissipation and peak load capacity. By combining an optimal slot length with an increased number of links, peak deformation can be increased by 50% without any loss in load capacity. Further investigations are underway to broaden the numerical database and rigorously validate these findings across a wider range of experiments.

6 ACKNOWLEDGEMENT

The authors would like to express their gratitude for the financial support provided by the Natural Sciences and Engineering Research Council of Canada (NSERC) through the Discovery Grant program.

7 REFERENCES

[1] T. Tannert and C. Loss, “Contemporary and Novel Hold-Down Solutions for Mass Timber Shear Walls,” *Buildings*, vol. 12, no. 2, p. 202, Feb. 2022, doi: 10.3390/buildings12020202.
[2] National Research Council of Canada (NRC), *National Building Code of Canada*, NRC, Ottawa, ON, Canada, 2015.
[3] Canadian Standards Association (CSA), *Engineering Design in Wood*, CSA Standard 086-24, CSA Group, Toronto, ON, Canada, 2024.
[4] C. Dickof, R. Jackson, H. Daneshvar, J. Nieder-Westberg, and Y. H. Chui, "Perforated plates as dissipative connections in timber seismic force resisting systems," in *Proceedings of WCTE 2021*, Santiago, Chile, 2021.
[5] M. Eatherton, J. Hajjar, G. Deierlein, H. Krawinkler, S. Billington, and X. Ma, "Controlled rocking of steel-framed buildings with replaceable energy-dissipating fuses," in *Proceedings of the 14th World Conference on Earthquake Engineering*, Beijing, China, 2008.

https://doi.org/10.52202/080513-0407

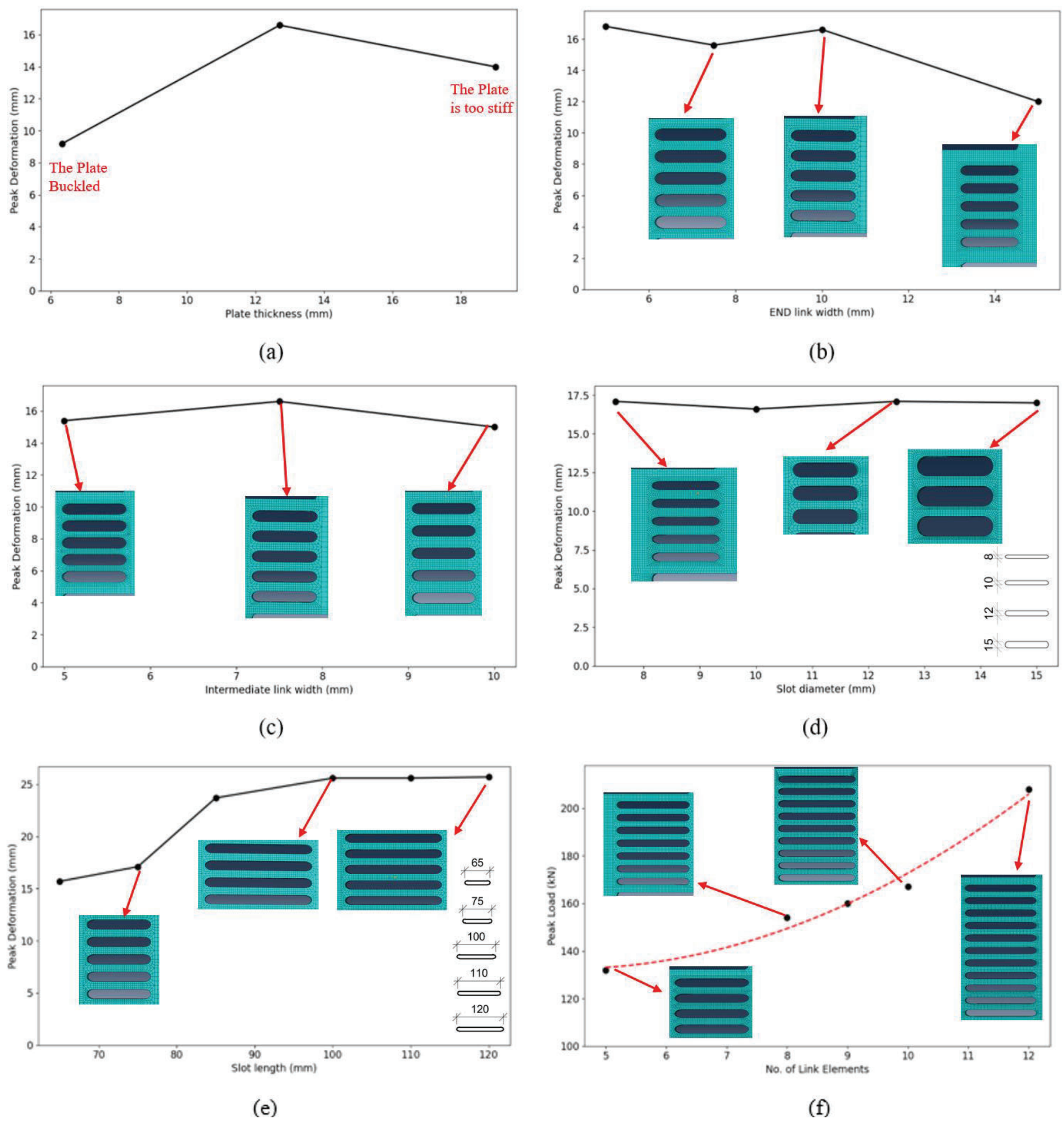

Figure 5. Peak Deformation for:(a) plate thickness, (b) end link width, (c) intermediate link width, (d) Slot diameter, (e)slot length.

And the Peak Load for: (f) the number of links.

[6] X. Ma, "Seismic design and behaviour of self-centering braced frame with controlled rocking and energy dissipating fuses," Ph.D. dissertation, Stanford University, Stanford, CA, USA, 2011.

[7] T. Kobori, Y. Miura, E. Fukuzawa, T. Yamada, T. Arita, Y. Taenaka, and T. Fukumoto, "Development and application of hysteresis steel dampers," in *Proceedings of the 10th World Conference on Earthquake Engineering*, Rotterdam, Netherlands, pp. 2341–2346, 1992.

[8] R. W. K. Chan and F. Albermani, "Experimental study of steel slit damper for passive energy dissipation," Engineering Structures, vol. 30, no. 4, pp. 1058–1066, Apr.2008,10.1016/j.engstruct.2007.07.005.

[9] D. R. Teruna, T. A. Majid, and B. Budiono, "Experimental Study of Hysteretic Steel Damper for Energy Dissipation Capacity," *Advances in Civil Engineering*, vol. 2015, pp. 1–12, 2015, doi: 10.1155/2015/631726.

[10] X. Zhang, M. Popovski, and T. Tannert, “High-capacity hold-down for mass-timber buildings,” *Construction and Building Materials*, vol. 164, pp. 688–703, Mar. 2018, doi: 10.1016/j.conbuildmat.2018.01.019.
[11] H.-E. Blomgren, S. Pei, J. Powers, J. Dolan, A. Wilson, and Z. Jin, "Cross-laminated timber rocking wall with replaceable fuses: Validation through full-scale shake table testing," in *Proceedings of WCTE 2018: World Conference on Timber Engineering*, Seoul, South Korea, 2018.
[12] I. Morrell, A. Phillips, J. Dolan, and H.-E. Blomgren, "Development of an inter-panel connector for cross-laminated timber rocking walls," in *Proceedings of WCTE 2018: World Conference on Timber Engineering*, Seoul, South Korea, 2018.
[13] S. Dires and T. Tannert, “Performance of coupled CLT shear walls with internal perforated steel plates as vertical joints and hold-downs,” *Construction and Building Materials*, vol. 346, p. 128389, Sep. 2022, doi: 10.1016/j.conbuildmat.2022.128389.
[14] H. Daneshvar, J. Niederwestberg, C. Dickof, R. Jackson, and Y. Hei Chui, “Perforated steel structural fuses in mass timber lateral load resisting systems,” *Engineering Structures*, vol. 257, p. 114097, Apr. 2022, doi:10.1016/j.engstruct.2022.114097.
[15] H. Daneshvar, Y. H. Chui, C. Dickof, and T. Tannert, “Experimental parametric study of perforated steel plate fuses for mass timber seismic force resisting systems,” *Journal of Building Engineering*, vol. 73, p. 106772, Aug. 2023,doi:10.1016/j.jobe.2023.106772.
[16] H. Daneshvar, J. Niederwestberg, J.-P. Letarte, and Y. Hei Chui, “Yield mechanisms of base shear connections for cross-laminated timber shear walls,” *Construction and Building Materials*, vol. 335, p. 127498, Jun.2022,doi:10.1016/j.conbuildmat.2022.127498.
[17] ABAQUS Inc., "ABAQUS Manual, Version 6.6," Providence, RI, USA, 2006.
[18] ASTM International, *Standard Test Methods for Cyclic (Reversed) Load Test for Shear Resistance of Vertical Elements of the Lateral Force Resisting Systems for Buildings*, ASTM E2126, West Conshohocken, PA, USA, 2018.

https://doi.org/10.52202/080513-0407